Published by IOP Publishing for Sissa Medialab

Received: *December 31, 2024*
Revised: *February 18, 2025*
Accepted: *March 7, 2025*
Published: *April 24, 2025*

Design and cosmic ray measurement of liquid scintillator tungsten slice ECAL for future collider

Hengyu Wang, Xiaojie Luo, Junguang Lv,* Xilei Sun and Manqi Ruan

Institute of High Energy Physics, Chinese Academy of Sciences
Beijing 100049, China
University of Chinese Academy of Sciences(UCAS)
Beijing 100049, China

E-mail: Lujg@ihep.ac.cn

Abstract: This study proposes a novel liquid scintillator-tungsten slice liquid medium electromagnetic calorimeter (ECAL). The design is based on the Shashlik structure, employing an ultra-thin liquid scintillator and tungsten slice alternate stacking strategy, aiming to achieve an excellent energy performance within limited space constraints for the future collider. Through Geant4 simulations, we have verified that the design has an energy resolution better than 5%@1GeV with a photoelectron yield of 100 p.e./mip, significantly superior to existing sampling calorimeter schemes. We fabricate a simple ECAL cell model and conducted cosmic ray tests, which achieve 170 p.e./mip and a 1% photonelectron collection and conversion efficiency. The mip signals compared between experimental and simulated demonstrated excellent consistency. Furthermore, the use of fast-emitting liquid scintillator as the sensitive material is expected to provide good timing performance, giving it the potential of a 5D calorimeter. This study not only provides a potential solution for future large collider experiments but also offers new ideas for the development of new calorimeters in other high-energy physics experiments.

Keywords: Calorimeters; Detector modelling and simulations I (interaction of radiation with matter, interaction of photons with matter, interaction of hadrons with matter, etc); Performance of High Energy Physics Detectors; Liquid detectors

*Corresponding author.

https://doi.org/10.1088/1748-0221/20/04/P04026

Contents

1 Introduction

With the discovery of the Higgs boson at the Large Hadron Collider (LHC) in 2012 [1, 2], precise measurements of its properties have become an important physics task in the field of particle physics. In the following decade, international efforts proposed the International Linear Collider (ILC) [3–8] and the Future Circular Collider (FCC) [9–12] as next-generation high-energy electron-positron colliders for precise measurements of the Higgs boson. Chinese physicists also proposed the Circular Electron Positron Collider (CEPC) [13–15] in 2012 as the next-generation Higgs factory, with the main physics goal of precise measurements of the Higgs boson and exploring the potential in electroweak physics. This requires a detector that can effectively reconstruct and distinguish the final decay states of the Higgs boson and intermediate vector bosons W, Z. In particular, for the physical process $H \to q\bar{q}, H \to W^+W^-/ZZ \to qq\bar{q}\bar{q}$. To achieve a good separation of W and Z bosons requires a mass resolution better than 4%. This demands a jet energy resolution of 3–4% at 100 GeV [13]. To achieve this goal, the CEPC adopts the Particle Flow Algorithm (PFA) [16, 17], which requires a calorimeter with high granularity and excellent energy resolution.

The electromagnetic calorimeter is primarily used for the precise measurement of the energy of decay-final-state photons in colliders, which is crucial for the reconstruction of physical processes. In the precise measurement of the decay of the $H \to \gamma\gamma$, an energy resolution of 20%@1GeV is sufficient to meet the requirements. Consequently, a silicon-tungsten sampling calorimeter [18] and a plastic scintillator-tungsten sampling calorimeter [19] scheme have been proposed for future colliders, achieving energy resolutions of 17%@1GeV [13] and 13%@1GeV [20], respectively. However, higher electromagnetic energy resolution is necessary in flavor physics and hadron spectroscopy

2025 JINST 20 P04026

research. This high resolution not only facilitates the efficient detection of low-energy photons or neutral pions in the decay processes of excited-state hadrons but also provides a more precise reconstruction of invariant mass, thereby effectively distinguishing between signals and backgrounds, as well as distinguishing events with similar final states and kinematic characteristics [21]. A BGO total absorption calorimeter [22] scheme was subsequently proposed. This scheme demonstrates exceptional performance in terms of energy resolution, achieving a resolution of 2–3%@1GeV. Nevertheless, the timing performance and costs may prove to be a challenge. One cost-effective option that balances performance and cost is the Shashlik calorimeter, which has been adopted by some international experiments. For example, in the KOPIO [23] and NICA-MPD experiments [24, 25], the calorimeters use an alternating arrangement of plastic scintillator and lead, connected by wavelength-shifting fibers. Both experiments have achieved energy resolutions better than $5\%/\sqrt{E}$. This design significantly improves the energy resolution, but it lacks longitudinal position resolution. This means that it cannot provide precise information on both energy and position simultaneously, which may have some impact on certain reconstruction algorithms and physics analyses. Furthermore, it occupies a large amount of space in longitudinal direction that makes it difficult to use in large collider experiments.

To overcome these limitations, this study proposes a new ECAL design based on a liquid scintillator. The design utilizes a strategy of alternating stacking of ultra-thin liquid scintillator layers with tungsten slices to optimize the calorimeter unit structure, significantly improving energy resolution and spatial positioning accuracy [26]. Through Geant4 simulations, we analyze in detail the physical and optical performance of this design at different energies and investigate the effects of various factors such as materials, thickness, and reflectivity on performance. Additionally, we set up an experimental platform to test the light collection performance of the ECAL unit and measure cosmic ray signals.

With the introduction of the 5D calorimeter concept, the demand for timing performance in ECAL is increasing. The 5D calorimeter requires not only precise spatial and energy information but also good timing resolution for particle flow reconstruction and event identification. This study uses fast scintillating liquid as the sensitive material, expecting to provide good timing performance and potential for a 5D calorimeter. This research not only offers a potential solution for the CEPC experiment but also provides new insights for the development of novel calorimeters in other high-energy physics experiments.

2 Conceptual design of the calorimeter structure

The primary design concept of our electromagnetic calorimeter (ECAL) is to achieve superior energy resolution within the confined spatial constraints of future colliders like CEPC, ILC, and FCC. This is accomplished by reducing the thickness of both the sensitive and absorber layers to the micrometer scale. By minimizing the thickness of the layers to hundreds of micrometers, sampling fluctuation is significantly reduced, that is a primary limiting factor in energy resolution for traditional sampling calorimeters. This innovative approach allows for a compact calorimeter design that can be integrated into the tight spatial requirements of advanced collider detectors while maintaining the high-resolution performance necessary for precise particle measurements.

Our ECAL is constructed from a novel arrangement of ultra-thin liquid scintillator layers and tungsten slices, forming a compact $2\,\text{cm} \times 2\,\text{cm} \times 2\,\text{cm}$ cubic unit, which is shown in figure 1. Each unit consists of 100 layers of liquid scintillator and 100 µm tungsten slice stacked alternately, creating a structure that optimizes the balance between material budget and energy resolution. Silicon

2025 JINST 20 P04026

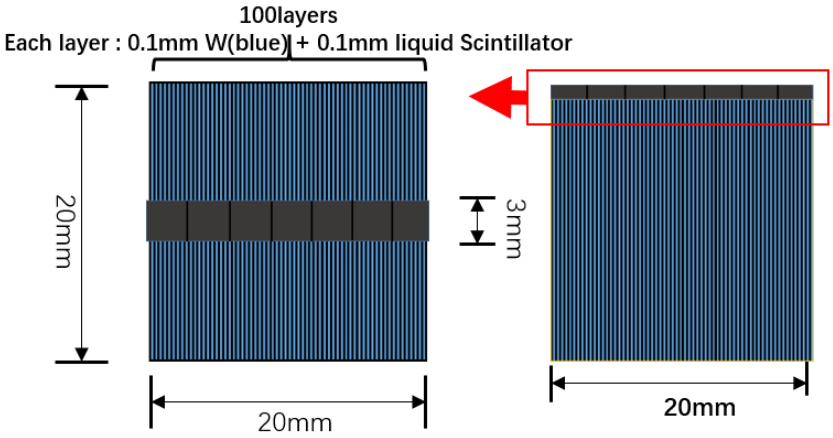

Figure 1. Schematic diagram of the liquid scintillator-tungsten thin slice electromagnetic calorimeter unit. The blue-black striped structure represents the alternating arrangement of liquid scintillator and tungsten slices, and the black strip represents the SiPM.

Photomultipliers (SiPMs) are used for readout from the side of the unit further ensures efficient photon collection, contributing to the overall performance of the ECAL.

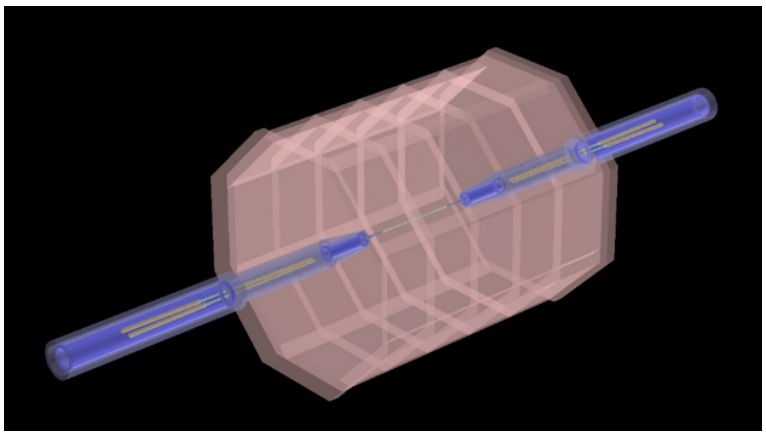

Figure 2. Schematic diagram of the overall structure of the liquid scintillator tungsten slice electromagnetic calorimeter. The blue represents the beam pipe, and the pink represents the outer appearance of the electromagnetic calorimeter structure.

The overall design of the ECAL is meticulously planned to align with the spatial and operational requirements of the CEPC, which inherits the baseline design of CEPC_V4 as shown in figure 2. The calorimeter comprises a barrel section and endcaps, tailored to fit within the collider's geometry without compromising the detection capabilities. The barrel section, with an inner radius of 1843 mm and a length of 4700 mm along the beam direction, is complemented by endcaps with a radius of 2088 mm [13]. The total inner surface area is approximately 80 m^2. The calorimeter is composed of 10 layers of 2 cm × 2 cm × 2 cm ECAL cell, with a total thickness of 20 *cm* in the longitudinal direction, approximately equivalent to 28 radiation lengths. The design also incorporates an extra 10 *cm* thick space reserved for the layout of electronics and future detector optimization.

2025 JINST 20 P04026

3 Simulation and performance

3.1 Geometry and simulation

In order to study the energy resolution of the calorimeter separately, we employed the Mokka [27] simulation toolkit under the CEPC software framework to construct a simplified geometry of the calorimeter module and performed Monte Carlo simulations to analyze the energy resolution. It is a 20 cm × 20 cm × 20 cm cube composed of 1000 of the aforementioned ECAL cells, with 10 ECAL cells in each direction of the three-dimensional space, which is shown in the figure 3.

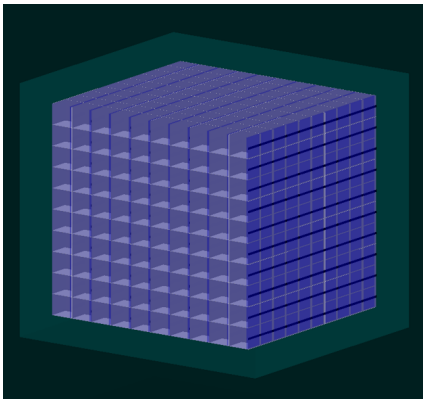

Figure 3. The ECAL module Geant4 geometry structure of the liquid scintillator tungsten slice electromagnetic calorimeter, which includes 10 cells in each dimension.

3.2 Monte Carlo simulation performance

To study the energy resolution performance of the ECAL module, the single gamma particles with energies ranging from 1 to 100 GeV were used as incident articles, which incident along the direction of the vertical tungsten plate. The intrinsic energy resolution, shown on the left side of figure 4, is close to ideal without the influence of noise. Therefore, a fit to the energy resolution was performed using $\frac{\sigma}{E} = \frac{a}{\sqrt{E}} \bigoplus c$, yielding an intrinsic energy resolution sampling term of 3.47%. The energy linearity plot on the right side of figure 4 reflects the energy leakage situation. It is important to note that the "Deposition energy" on the vertical scale of the right figure refers to the energy deposited in the liquid scintillator. With the overall thickness of the ECAL module reaching 28 X_0, energy leakage is minimal, resulting in an overall energy non-linearity better than 3%.

The sampling fraction directly affects the energy resolution, Therefore, we studied the impact of three different sensitive materials, liquid scintillator (LS), scintillating glass (Glass), and cesium iodide crystal (CsI), on the energy resolution of the calorimeter using Geant4 simulations, as shown in figure 5, with corresponding sampling fractions of 0.072, 0.146, 0.197, and 0.292.

The detailed simulation of the ECAL structure and the simulation results are listed in table 1, demonstrate that the calorimeter's intrinsic energy resolution can be significantly enhanced by the choice of sensitive material. When using a 100 µm liquid scintillator and 100 µm tungsten ECAL structure, the intrinsic energy resolution of the calorimeter is 3.5% at 1 GeV. If the liquid scintillator is replaced with heavier materials such as scintillating glass and cesium iodide crystal, the ECAL intrinsic energy resolution is 2.8% at 1 GeV and 2.5% at 1 GeV, respectively. If a thicker layer of cesium iodide crystal is used as the sensitive layer, the ECAL intrinsic energy resolution can reach a 2% level.

2025 JINST 20 P04026

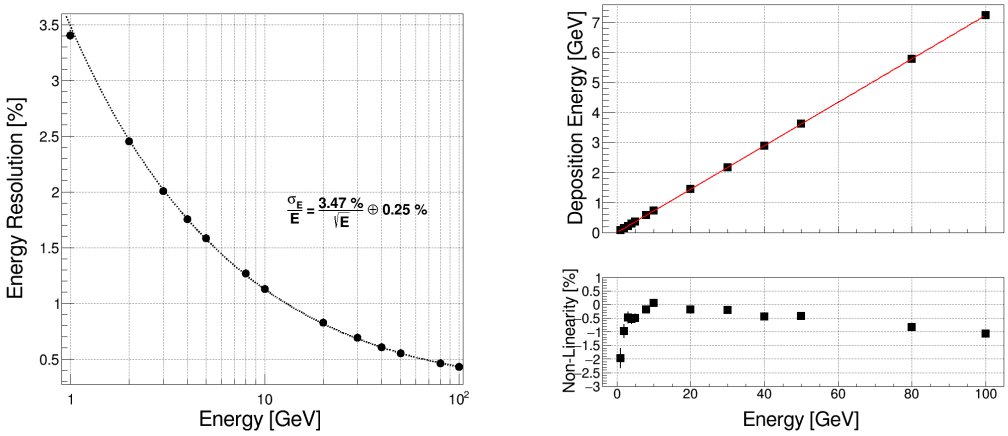

Figure 4. Intrinsic energy resolution and energy linearity of LS-W ECAL. The vertical axis of the right plot represents the energy deposited in the liquid scintillator.

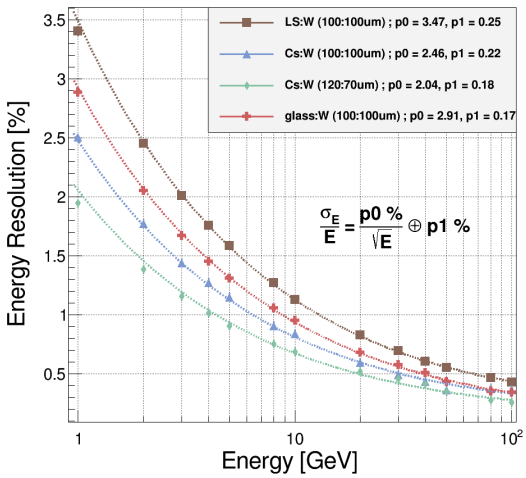

Figure 5. Intrinsic energy resolution of ECAL with different sensitive materials. The black line, blue line, and red line correspond to a 100 µm thick tungsten absorber, with sensitive materials of 100 µm thick liquid scintillator, 100 µm thick scintillating glass, and 100 µm thick cesium iodide crystal, respectively. The purple line represents the energy resolution results when using a 120 µm thick cesium iodide crystal as the sensitive material, while reducing the thickness of the tungsten absorber to 70 µm.

Table 1. Sampling term of energy resolution in different ECAL structure.

ECAL Structure	Sampling Fraction	Sampling Term(%)
LS: W = 100 µm:100 µm	0.072	3.47
Glass: W = 100 µm:100 µm	0.146	2.91
CsI: W = 100 µm:100 µm	0.197	2.46
CsI: W = 120 µm:70 µm	0.292	2.09

2025 JINST 20 P04026

3.3 Digitization

The energy and position information of the incident particles is obtained through the interaction between the incident particles and the liquid scintillator, which generates scintillation photons. These photons are then propagated through the liquid scintillator in the calorimeter cell and eventually collected by the SiPMs located at the end, where they are converted into photoelectrons. The number of photons collected by the SiPMs follows a Poisson distribution. This Poisson distribution introduces an additional fluctuation to the energy resolution of the ECAL. In addition, the gain of the SiPM and electronic noise also contribute to additional fluctuations in the energy resolution. The method used to quantify the fluctuation in the energy resolution of the calorimeter caused by optical and electronic system is the digitization process.

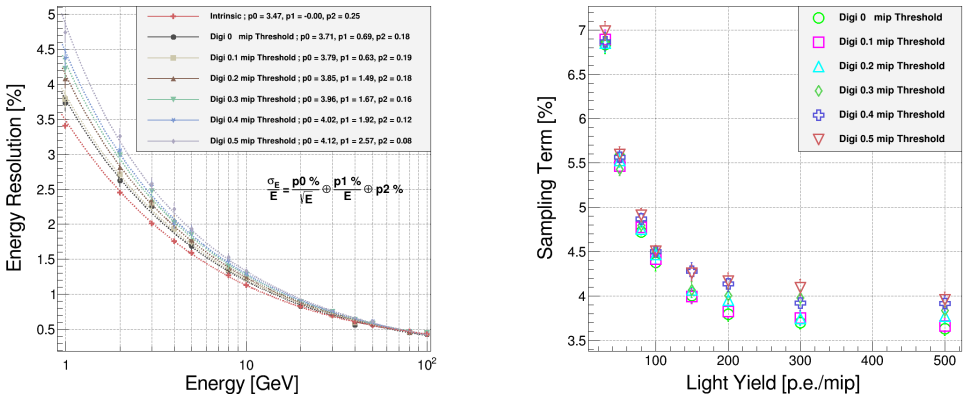

Figure 6. ECAL Energy Resolution at 200 p.e./mip photoelectron yield (Left), MC Simulation Results of the Relationship between ECAL Energy Resolution Sampling Term and photoelectron yield (Right).

The performance of the ECAL with a structure of 100 µm liquid scintillator and 100 µm tungsten was simulated using Mokka. The results after digitization processing were shown in the left of figure 6. Under a photoelectron yield of 200 p.e./mip, the energy resolution of ECAL is around 4-5% at a energy threshold below 0.5 mip. The value of the photoelectron yield directly affects the digitization results, and a sufficiently large photoelectron yield makes the digitization results closer to the intrinsic energy resolution. The right of figure 6 displays the distribution of the sampling term of the ECAL energy resolution for different numbers of collected photoelectrons by the SiPMs. When the photoelectron yield is 80 p.e./mip, the sampling term of the ECAL energy resolution is around 4.5%. As the vaule of photoelectron yield increases, the sampling term of the ECAL energy resolution decreases and tends to flatten. In the case of 500 p.e./mip, the sampling term of the ECAL energy resolution will be better than 4%.

3.4 Optical simulation

From figure 6, it is evident that the number of photoelectrons collected by the SiPM has a significant impact on the energy resolution of the ECAL. To achieve the desired performance of $5\%/\sqrt{E}$ for the calorimeter design, a conservative estimate for the photoelectron yield per ECAL unit is around 100 p.e./mip. In order to optimize the optical performance and design the optimal optical conditions to ensure that the calorimeter performance achieves the design specifications, Geant4 optical simulations

2025 JINST 20 P04026

on different optical conditions for the tungsten slice surfaces have been researched. The basic geometric structure is illustrated in figure 7, where the gray-white cubic cells represent the alternately arranged liquid scintillator and tungsten slices in the ECAL unit. ESR (Enhanced Specular Reflector) films, which are designed to maximize light reflection and minimize light loss, are applied to five sides of the ECAL unit. These films help to enhance the overall light collection efficiency within the detector. The surfaces of the tungsten slices are set with different reflectivities. The blue transparent thin sheet represents the organic glass used as a transparent window, and the black strip on the outside represents the SiPM with a photon-to-electron conversion efficiency of 25%.

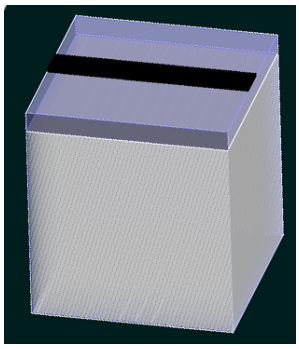

Figure 7. Geant4 schematic diagram of the optical simulation structure of the liquid scintillator tungsten slice electromagnetic calorimeter.

Due to the extremely thin layer structure of the liquid scintillator, scintillation light needs to undergo multiple reflections in the liquid scintillator before reaching the surface of the SiPM. Excessive reflection causes significant attenuation of the scintillation light, resulting in very few photoelectrons collected by the SiPM. We conducted a detailed study on the effects of the surface reflectivity of the tungsten slcies, the granularity of the ECAL unit, and the thickness of the liquid scintillator on the optical performance, with detailed results shown in the figure 8. For an ECAL cell size of 20 mm, the number of photoelectrons corresponding to an 80% reflectivity is less than 20 p.e./mip. Increasing the reflectivity results in a nearly exponential increase in the number of photoelectrons collected by the SiPM. To achieve the expected 100 p.e./mip, the required surface reflectivity of the tungsten slices is around 96%. Reducing the ECAL cell size improves the optical performance, If the ECAL cell size is reduced to 10 mm, the required reflectivity for 100 p.e./mip decreases to 93%. Additionally, the optical performance improves with an increase in the thickness of the liquid scintillator. With a fixed 95% reflectivity, for an ECAL cell size of 20 mm, achieving the expected 100 p.e./mip corresponds to a liquid scintillator thickness of 120 µm.

One of the key challenges in achieving high photoelectron yield is the attenuation of scintillation light due to multiple reflections within the thin liquid scintillator layer. To address this, we proposed an extra thin layer of air as a total internal reflection layer on the surface of the tungsten slices in Geant4, which significantly improved the optical performance. The simulation results, as detailed in table 2. With surface reflectivities of 80%, 90%, 95%, and 100% on the tungsten slices, the corresponding number of photoelectrons increased to 414, 677, 986, and 1814 p.e./mip, respectively.

It is important to note that while the implementation of a Total Internal Reflection (TIR) layer is currently challenging, advancements in manufacturing technology may make this design feasible in the future. One promising approach involves wrapping a thin layer of plastic film on the surface of the tung-

2025 JINST 20 P04026

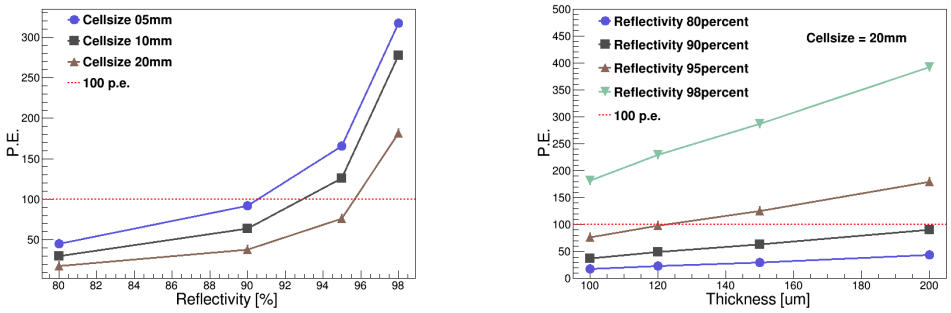

Figure 8. The relationship between the number of photoelectrons collected by the SiPM and the surface reflectivity (left) of the tungsten slices, as well as the thickness of the liquid scintillator (right).

Table 2. Photoelectron yield in different tungsten surface reflectivity.

reflectivity (%)	photoelectron yield (p.e./mip)
80	414
90	677
95	986
100	1814

sten slices, with a micron-level air layer between the plastic film and the tungsten slice. Additionally, in recent years, with the development of material technology, low-refractive-index silicon dioxide coatings have also become one of the ways to achieve the design of a total internal reflection layer [28–30].

In conclusion, the optical simulation results provide valuable insights into optimizing the ECAL's optical performance and highlight the potential of innovative solutions like the TIR layer to achieve the stringent requirements of future collider experiments.

3.5 π^0/γ identification

Understanding the detector's capability to distinguish between π^0 and γ is essential for evaluating its physical performance in high-energy physics experiments [31]. Generally, a smaller granularity of ECAL correlates with improved performance, resulting in a larger number of corresponding electronic readout channels. To strike a balance between electronic complexity and detector performance, a granularity of $2\,\text{cm} \times 2\,\text{cm} \times 2\,\text{cm}$ has been selected for the ECAL at $5\%/\sqrt{E}$. This section focuses on assessing the appropriateness of this granularity by quantifying the identification performance of the ECAL with a granularity of $2\,\text{cm} \times 2\,\text{cm} \times 2\,\text{cm}$ for π^0 and γ events.

There are two types of π^0 event in ECAL reconstruction, one type is "resolved" π^0, which from two separate double-gamma clusters, the other type is "merged" π^0, which from a single merged double-gamma cluster. For the "resolved" π^0, it can be easily reconstructed by two separated gamma clusters [14]. However, for merged π^0, as the two gamma clusters are too close in the ECAL, they cannot be recognized as two separate clusters and are instead considered as one cluster. Therefore, in such cases, it is necessary to determine whether the merged cluster is from a π^0 or a high-energy gamma. A simple study was conducted to address this issue.

2025 JINST 20 P04026

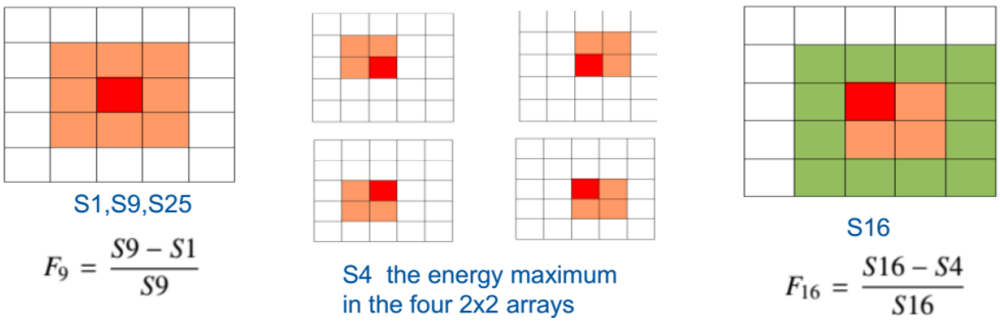

Figure 9. The definitions of S1, S4, S9, S16, S25, and F9, F16.

Firstly, several parameters were defined. S1 represent the hit at the energy center position of a certain layer in ECAL, and the surrounding four, nine, sixteen, or twenty-five hits are defined as S4, S9, S16, and S25, and corresponding definitions of F9 and F16 are shown in figure 9.

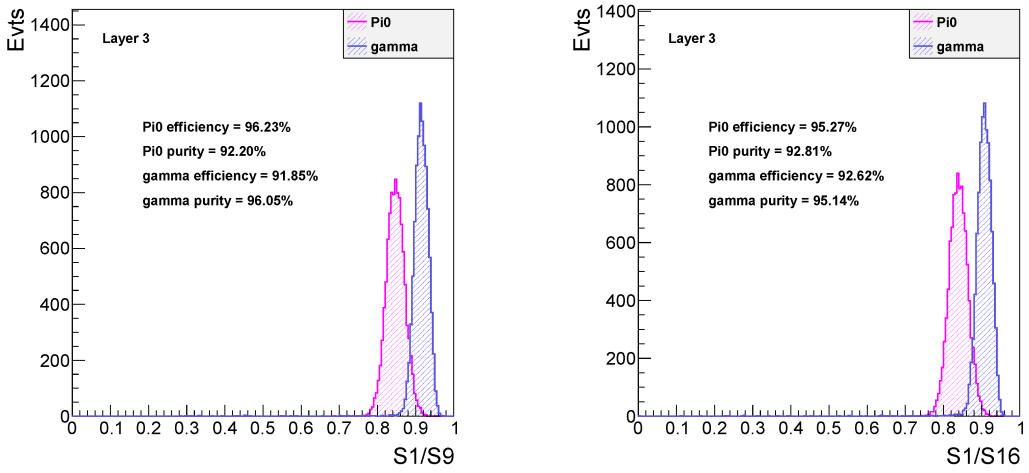

Figure 10. π^0 and γ identification efficiency and purity with S1/S9 and S1/S16.

Samples of 40 GeV merged π^0 and 40 GeV γ were used to study the identification power of ECAL for π^0 and γ events. The double-gammas from the merged π^0 were set to hit the same cell in ECAL at a distance of 1 cm. The information of parameters S1, S4, S9, S16 at the layer with the maximum lateral spread of the cluster (third layer) in ECAL was used for π^0 and γ identification, as shown in the figure 10. It was found that using S1/S9 and S1/S16 could effectively distinguish merged π^0 from γ events, with π^0 identification efficiencies of 96.23% and 95.27%, and corresponding purity of 92.20% and 92.81% with a ECAL resolution at $5\%\sqrt{E}$. Efficiency is defined as $eff_{\pi^0} = \frac{\pi^0_{\text{Selected}}}{\pi^0_{\text{All}}}$, and purity is defined as $purity_{\pi^0} = \frac{\pi^0_{\text{Selected}}}{\pi^0_{\text{Selected}}+\gamma_{\text{Selected}}}$. It is important to note that in future collider experiments, over 90% of π^0 energies are expected to be below 40 GeV. Therefore, the ability to distinguish 40 GeV π^0 sufficiently demonstrates that the selected granularity of the ECAL is adequate for effective particle identification in realistic experimental conditions.

2025 JINST 20 P04026

4 Experiment

4.1 Experimental equipment

The H10828 model PMT purchased from HAMAMATSU was used as the light detection device, featuring a circular photocathode surface with a diameter of 34 mm. Two channels of EQR10 11-3030D-S model SiPM purchased from NDL coupled to plastic scintillator tile as the triggering device, powered by ORTEC 556 HIGH VOLTAGE POWER SUPPLY and ORTEC 710 QUAD BIAS SUPPLY respectively, and signal acquisition was done using PicoScope 5000 Series oscilloscope. The liquid scintillator is from JUNO experiment and contain 2.5 g/L 2,5-diphenyloxazole (PPO) as the fluor and 3 mg/L p-bis-(o-methylstyryl)-benzene (bis-MsB) as the wavelength shiter [32].

4.2 Single photon calibration

Before the ECAL optical performance test, The single photon response for PMT need to be calibrated. The method is to output two pulse signals from the signal generator, with one 6.7 V pulse signal sent to the LED as a pulse light source, and the other 0.8 V synchronized NIM signal as the trigger signal for the oscilloscope. When the LED emits light upon receiving the pulse signal from the signal generator, the oscilloscope simultaneously receives the trigger signal to start collecting waveforms. Which was shown in the left of figure 11. By adjusting the pulse intensity to make the LED emit weak light so that the PMT can only receive single photon signals, data analysis can be used to calibrate the single photon signal.

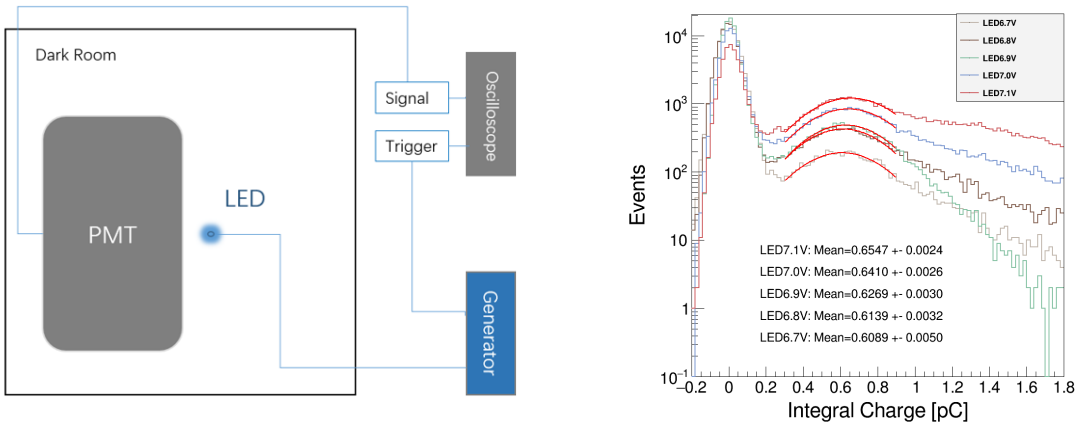

Figure 11. Single photon testing platform schematic diagram (left), and integral charge of the single photon response (right).

The voltage generated by the signal generator gradually increased from 6.7 V to 7.1 V, and the integral charge collected by the oscilloscope is shown in the right of figure 11. The unit of integral charge is picocoulomb, which is 10^{-12} C, and the vertical axis is in event counts. Using a Gaussian distribution to fit the peak positions of the integral signals at different voltages, the single photoelectron signal was obtained. The minimum voltage of 6.7 V corresponds to a single photon integral charge of 0.6089 pC.

2025 JINST 20 P04026

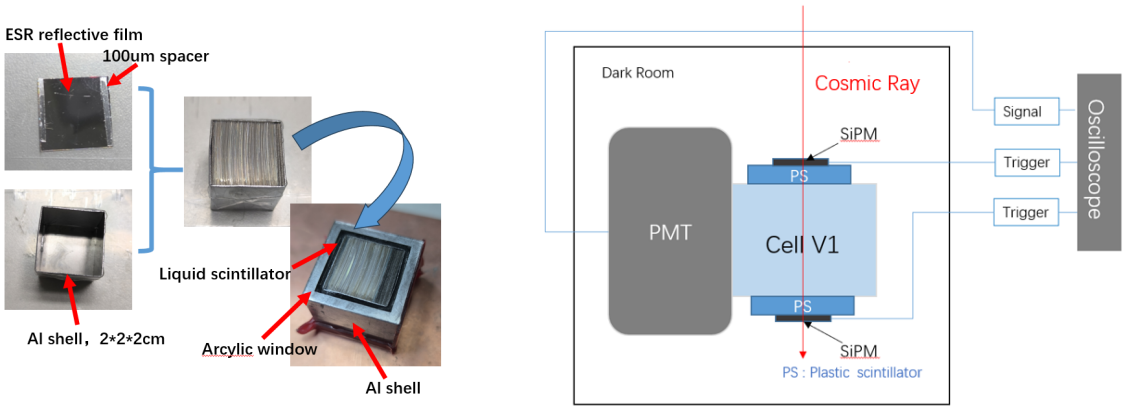

Figure 12. Fabrication of ideal optical model ECAL Cell_V1 (left), and cosmic ray test platform (right).

4.3 ECAL Cell optical performance and cosmic ray signals

ESR reflective film was used to fabricate a ECAL cell model Cell_V1 for optical performance test and cosmic ray signal measurement. The specific fabrication method is shown in the left of figure 12, where the ESR film is first cut into 2 cm^2 pieces, with a thickness 100 µm plastic spacer placed on both sides of the ESR film as a gap for filling the liquid scintillator. An 2 cm^3 aluminum shell is made as a container and leaving one side as the optical output window. The ESR film with the spacer is then placed into the aluminum shell one by one, forming a structure with alternating ESR film and 100 µm gaps, and the optical window is sealed with acrylic organic glass. Finally, it is immersed in the liquid scintillator to form the ECAL Cell_V1 as shown in the figure 12. The current experiment and the ECAL cell model primarily focus on measuring optical performance and cosmic ray signals. Cosmic ray particles are relativistic muons and electrons that are Minimum Ionizing particles (MIP) that do not produce significant clustering effects. The tungsten sheets serve only as absorbers and have minimal impact on the observed signals. Therefore, we have not included tungsten sheets as the absorbers at this stage. A more comprehensive and detailed ECAL model will be developed and refined in future experiments.

The experimental setup of the optical performance and cosmic ray signals test is shown in the right of figure 12. SiPM-coupled plastic scintillators were used as the trigger the top and bottom of the ECAL cell, and the optical window of the ECAL cell was directly coupled to the PMT window with silicone oil. When a cosmic ray signal passed through the ECAL cell, both plastic scintillators triggered simultaneously, and the oscilloscope started collecting signals. The area of the trigger SiPM is 1 cm^2 so the cosmic ray is not extremely vertical, this fluctuation is not be corrected in this experiment. The cosmic ray measurement results are shown in the left of figure 13, and fitting with a convolution of the Landau distribution and Gaussian distribution showed a peak position at 103.9 pC, with a Landau width and Gaussian width of sigma = 11.21 pC and sigma = 9.009 pC, respectively. The MPV value of 103.9 pC corresponds to 170 p.e., the photoelectron yield of the liquid scintillator is 17000 p.e., and the corresponding total photoelectron efficiency is 1%.

In this experiment, a PMT was used for optical readout, covering the entire optical window (20 mm × 20 mm) of the ECAL cell, resulting in a detection of 170 p.e. In the simulation, a 3 mm × 20 mm SiPM array was used for readout and yielded 182 p.e. The main difference between the two readout methods lies in the coverage of the optical area. We adjusted the width of the SiPM in

2025 JINST 20 P04026

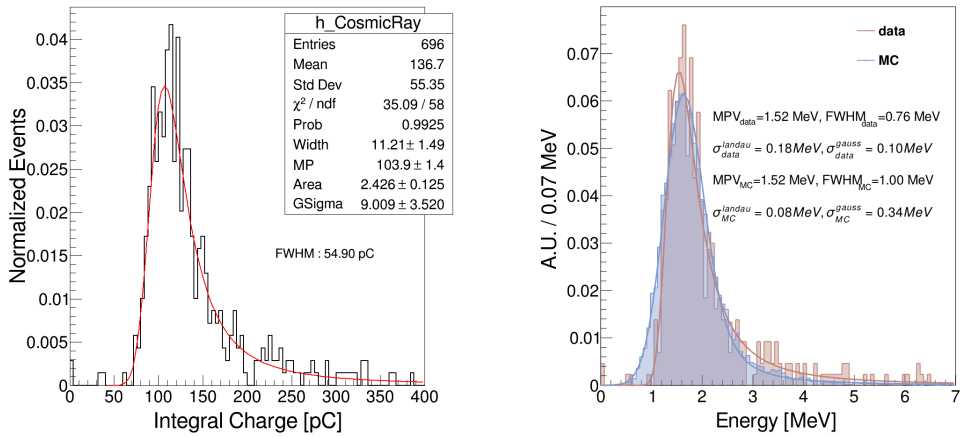

Figure 13. The original cosmic ray measurement results (left) and mip energy compared with cosmic ray result and Geant4 simulation (right).

the simulation to match the PMT size of 20 mm, yielding 624 p.e. This indicates that, due to area effects, the expected optical performance of the SiPM shows about a 3.4-fold reduction. However, better photon detection efficiency (PDE) of SiPM would mitigate this value.

Although the simulation predicted a higher yield of photoelectrons, the experimental results demonstrated lower values. This phenomenon is mainly attributed to the blocking of photon propagation by the spacers used in the experiment, along with the simple manufacturing conditions, which made it difficult to meet the reflective conditions assumed in the simulation, further decreasing light collection efficiency and consequently affecting the photoelectron yield. Nevertheless, as a preliminary experimental result, it is sufficient to demonstrate the feasibility of the approach. To more accurately evaluate these optical performances and improve the photoelectron yield, we plan to conduct more refined experimental studies, including ultra-thin total reflection film fabrication processes, optimization of SiPM array area and layout schemes, and new optical collection schemes.

To further compare the consistency between experimental results and simulated expectations, we calibrated the cosmic ray signals to minimum ionizing particle (mip) signals and normalized them for comparison with the Geant4 simulated MIP signals, as shown in the right panel of figure 13. The Geant4 results were digitized with 170 p.e./mip. The results indicate that the experimental and simulated mip signals matched well. And the energy distribution FWHM of cosmic ray mip signal is slightly smaller than the simulation results, that indicates the performance of experiment mip signal is better than simulation. This discrepancy is attributed to a relatively conservative digitization model, which ensures that subsequent experimental results can meet the expected performance of the simulation.

4.4 Prospects and possibilities ahead

The current liquid scintillator-tungsten slice ECAL design shows impressive performance, but there are still many opportunities for improvement. This design is considered a conservative transitional solution. Future exploration of liquid medium slice ECAL can take two main directions: investigating total internal reflection materials [28–30] combined with high-luminescence scintillating materials [33] to significantly enhance light collection and readout efficiency; developing organic perovskite thin

2025 JINST 20 P04026

films as sensitive materials [34, 35], which may offer better performance and enable innovative detection methods in calorimeter design.

5 Conclusion

This study presents a comprehensive design and evaluation of a novel liquid scintillator-tungsten slice electromagnetic calorimeter (ECAL) for future collider. The primary goal was to develop a spatially compact sampling electromagnetic calorimeter with high granularity and excellent energy resolution by reducing the thickness of the sensitive and absorber layers to the order of hundreds of micrometers to reduce sampling fluctuations.The basic design of an ECAL unit structure consists of alternating layers of 100 µm thick liquid scintillator and 100 µm thick tungsten, and the sampling ratio of the ECAL is 0.072. Geant4 simulation has demonstrated that the proposed ECAL design achieved an energy resolution better than $5\%/\sqrt{E}$, with a photoelectron yield of 100 p.e./mip for the ECAL cell, and the intrinsic energy resolution is $3.47\%/\sqrt{E}$. This represents a significant improvement over existing sampling calorimeter schemes.

Geant4 simulation has quantified the optical performance of the ECAL unit. To achieve an energy resolution better than $5\%/\sqrt{E}$, the photoelectron yield of the ECAL cell needs to conservatively reach 100 p.e./mip. This requirement can be achieved with a reflectivity of 96% for the reflection layer on the tungsten slice surface. Moreover, the incorporation of a TIR film on the tungsten surface could excellently enhance the optical performance, allowing the ECAL cell to achieve a photoelectron yield exceeding 500 p.e./mip with a tungsten slice surface reflectivity of 90%.

An ECAL cell module was fabricated, And the optical performance and cosmic ray signals have been measured. The experimental results showed a photoelectron yield of 170 p.e./mip at a 98% reflectivity and a total photoelectron efficiency of 1%. The mip signals of experiment and simulation matched well, which demonstrated excellent consistency between experiment and simulation and confirmed the ECAL's performance, showcasing its potential for using in future collider experiments.

The innovative design of our ECAL, with its "layer-cake" structure and potential for 5D calorimetry, offers a promising solution for future collider experiments. While challenges remain in achieving the full potential of the design, particularly in optimizing the optical performance, advancements in material technology and manufacturing processes offer avenues for future improvements. This research provides a foundation for the development of next-generation calorimeters for high-energy physics research, contributing to the advancement of experimental techniques and detector technology in the field.

References

[1] ATLAS collaboration, *Observation of a new particle in the search for the Standard Model Higgs boson with the ATLAS detector at the LHC*, *Phys. Lett. B* **716** (2012) 1 [arXiv:1207.7214].

[2] CMS collaboration, *Observation of a New Boson at a Mass of 125 GeV with the CMS Experiment at the LHC*, *Phys. Lett. B* **716** (2012) 30 [arXiv:1207.7235].

[3] B. List, L. Hagge, J. Kreutzkamp and N. Walker, *Design Integration at the International Linear Collider*, in the proceedings of the *4th International Particle Accelerator Conference*, Shanghai, China, May 12–17 (2013).

[4] T. Behnke et al., *The International Linear Collider Technical Design Report - Volume 1: Executive Summary*, arXiv:1306.6327.

2025 JINST 20 P04026

[5] ILC collaboration, *The International Linear Collider Technical Design Report — Volume 2: Physics*, arXiv:1306.6352.

[6] C. Adolphsen et al., *The International Linear Collider Technical Design Report — Volume 3.I: Accelerator & in the Technical Design Phase*, arXiv:1306.6353.

[7] C. Adolphsen et al., *The International Linear Collider Technical Design Report — Volume 3.II: Accelerator Baseline Design*, arXiv:1306.6328.

[8] H. Abramowicz et al., *The International Linear Collider Technical Design Report — Volume 4: Detectors*, arXiv:1306.6329.

[9] FCC collaboration, *FCC Physics Opportunities: Future Circular Collider Conceptual Design Report Volume 1*, *Eur. Phys. J. C* **79** (2019) 474.

[10] FCC collaboration, *FCC-ee: The Lepton Collider: Future Circular Collider Conceptual Design Report Volume 2*, *Eur. Phys. J. ST* **228** (2019) 261.

[11] FCC collaboration, *FCC-hh: The Hadron Collider: Future Circular Collider Conceptual Design Report Volume 3*, *Eur. Phys. J. ST* **228** (2019) 755.

[12] FCC collaboration, *HE-LHC: The High-Energy Large Hadron Collider: Future Circular Collider Conceptual Design Report Volume 4*, *Eur. Phys. J. ST* **228** (2019) 1109.

[13] CEPC Study Group collaboration, *CEPC Conceptual Design Report: Volume 2 — Physics & Detector*, arXiv:1811.10545.

[14] CEPC Study Group collaboration, *CEPC Conceptual Design Report: Volume 1 — Accelerator*, arXiv:1809.00285.

[15] CEPC Study Group collaboration, *CEPC Technical Design Report: Accelerator*, *Radiat. Detect. Technol. Methods* **8** (2024) 1 [arXiv:2312.14363].

[16] J.-C. Brient, *Improving the Jet Reconstruction with the Particle Flow Method; an Introduction*, physics/0412149 [DOI:10.1142/9789812701978_0056].

[17] M. Ruan and H. Videau, *Arbor, a new approach of the Particle Flow Algorithm*, in the proceedings of the *International Conference on Calorimetry for the High Energy Frontier*, Lyon, France, October 2–6 (2017) [arXiv:1403.4784].

[18] K. Kawagoe et al., *Beam test performance of the highly granular SiW-ECAL technological prototype for the ILC*, *Nucl. Instrum. Meth. A* **950** (2020) 162969 [arXiv:1902.00110].

[19] CALICE collaboration, *The Scintillator-ECAL Beam Test at DESY, 2007 — Update 3*, CALICE Analysis Note CAN-012 (2008).

[20] CALICE collaboration, *The Scintillator-ECAL Beam Test at DESY, 2007 — First results*, CALICE Analysis Note CAN-005 (2007).

[21] Y. Wang et al., *Prospects for $B^0_{(s)} \to \pi^0\pi^0$ and $B^0_{(s)} \to \eta\eta$ modes and corresponding CP asymmetries at Tera-Z*, *JHEP* **12** (2022) 135 [arXiv:2208.08327].

[22] CEPC Calorimeter Working Group collaboration, *A novel high-granularity crystal calorimeter*, *PoS* **ICHEP2022** (2022) 348.

[23] G.S. Atoian et al., *Development of Shashlyk calorimeter for KOPIO*, *Nucl. Instrum. Meth. A* **531** (2004) 467 [physics/0310047].

[24] V.V. Kulikov et al., *ECAL MPD: geometry and simulation*, 2020 *JINST* **15** C09017.

[25] Y. Li et al., *Production and quality control of NICA-MPD shashlik electromagnetic calorimeter in Tsinghua University*, 2022 *JINST* **17** T04005.

2025 JINST 20 P04026

[26] R. Wigmans, *Calorimetry: Energy measurement in particle physics*, Oxford University Press (2017) [DOI:10.1093/oso/9780198786351.001.0001].

[27] P. Mora de Freitas and H. Videau, *Detector simulation with MOKKA / GEANT4: Present and future*, in the proceedings of the *International Workshop on Linear Colliders (LCWS 2002)*, Jeju Island, South Korea, August 26–30 (2002), pp. 623–627.

[28] H. Wu et al., *Nanoporous Silicon Dioxide Films for Large Area and Low-Cost Fabrication of Ultra-Low Refractive Index Coatings*, *ACS Appl. Nano Mater.* **6** (2023) 15437.

[29] N. Tajima, H. Murotani and T. Matsudaira, *Optical multicoating using low-refractive-index SiO2 optical thin films deposited by sputtering and electron beam evaporation*, *Thin Solid Films* **776** (2023) 139824.

[30] M.R. Krishnan, V. Rajendran and E. Alsharaeh, *Anti-reflective and high-transmittance optical films based on nanoporous silicon dioxide fabricated from templated synthesis*, *J. Noncryst. Solids* **606** (2023) 122198.

[31] M. Calvo Gomez et al., *A tool for γ/π^0 separation at high energies*, LHCb-PUB-2015-016 (2015).

[32] JUNO collaboration, *JUNO physics and detector*, *Prog. Part. Nucl. Phys.* **123** (2022) 103927 [arXiv:2104.02565].

[33] X. Du et al., *Efficient and ultrafast organic scintillators by hot exciton manipulation*, *Nature Photon.* **18** (2024) 162.

[34] P. Jin et al., *Realizing nearly-zero dark current and ultrahigh signal-to-noise ratio perovskite X-ray detector and image array by dark-current-shunting strategy*, *Nature Commun.* **14** (2023) 626.

[35] X. Ou and F. Gao, *Blossoms in perovskite planar X-ray detectors*, *Nature Commun.* **15** (2024) 5754.

2025 JINST 20 P04026